Poroelastic stress triggered seismic activity in the Changning shale gas hydraulic fracturing region, Sichuan Basin, China

Wei Tao[1], Renqi Lu[2], Dengfa He[3], Jianbao Sun[1], Yuxin Bao[1], Yiduo Liu[4], Guixi Yi[5], Yan Zhan[1], Weikang Zhang[6], and Guangshen Liu[1]

[1]State Key Laboratory of Earthquake Dynamics, Institute of Geology, China Earthquake Administration
[2]Institute of Geology, China Earthquake Administration, Beijing 100029, China.
[3]School of Energy Resources, China University of Geosciences Beijing
[4]University of Houston
[5]Earthquake Administration of Sichuan Province
[6]College of Energy Resources, China University of Geosciences

November 23, 2022

Abstract

The recent increase in the seismic activity in the southern Sichuan Basin, China, is potentially related to shale gas hydraulic fracturing. However, the detailed mechanism of hydraulic fracturing requires further verification. In this study, high-resolution seismic profiles are used to reveal several large pre-existing faults in the basement. Based on the fully coupled poroelastic theory, we calculate the perturbing poroelastic stress field caused by hydraulic fracturing using a finite element model constrained by well-defined geological data, detailed injection data, and radar data. The results indicate that the small earthquakes are correlated with the distribution of the poroelastic stress, which is concentrated and extends a large distance along the weak stratum in the sediment beyond the fluid diffusion. Two moderate earthquakes are consistent with the increase of the Coulomb's stress in spatial-temporal evolution; thus, they are likely triggered earthquakes resulting from the reactivation of deep pre-existing faults.

Hosted file

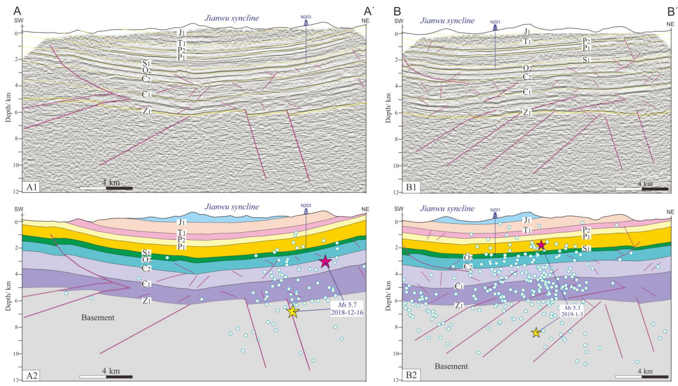
A
A′
B
B′
SW
NE
Jianwu syncline
Depth/ km
A1
B1
A2
B2
4 km
Basement
Ms 5.7
2018-12-16
Ms 5.3
2019-1-3

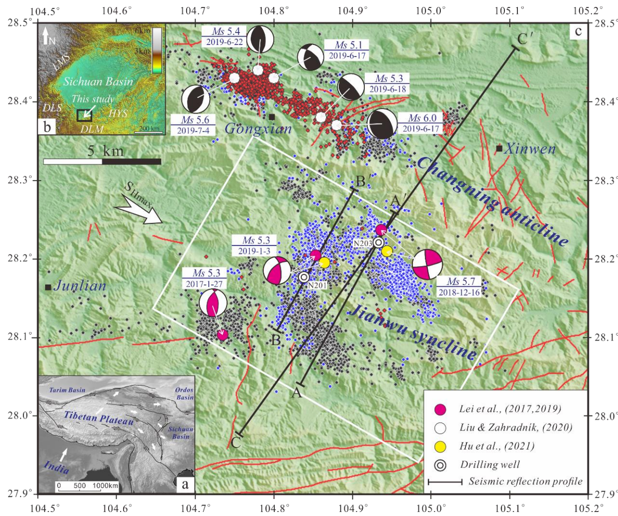

Ms 5.4
2019-6-22
Ms 5.1
2019-6-17
Ms 5.3
2019-6-18
Ms 5.6
2019-7-4
Ms 6.0
2019-6-17
Gongxian
Xinwen
Changning anticline
Ms 5.3
2019-1-3
Ms 5.3
2017-1-27
Ms 5.7
2018-12-16
Junlian
Jianwu syncline
N203
N201
Sichuan Basin
This study
5 km
Tibetan Plateau
Tarim Basin
India
Lei et al., (2017,2019)
Liu & Zahradnik, (2020)
Hu et al., (2021)
Drilling well
Seismic reflection profile

Coulomb Stress Evolution

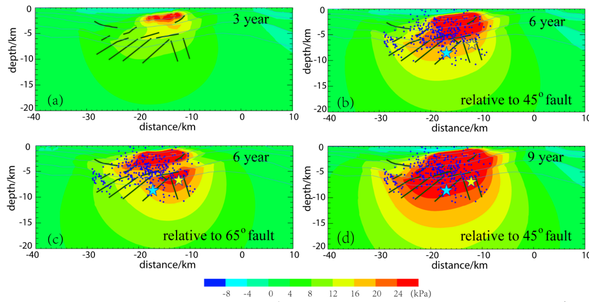

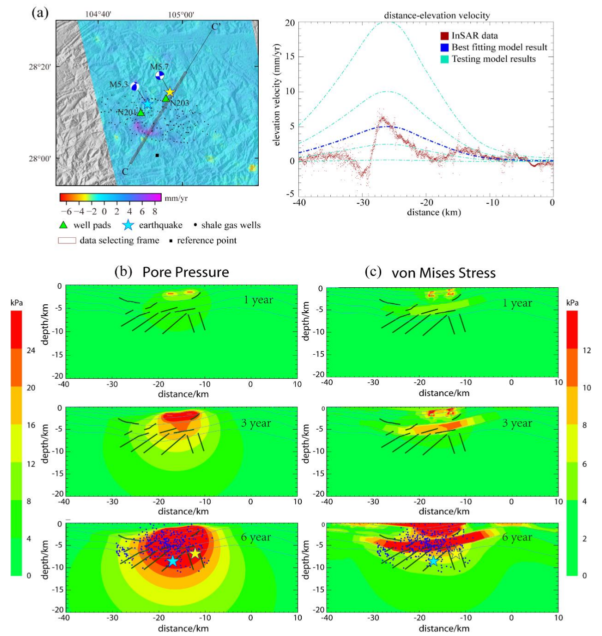
(a)
104°40'
105°00'
28°20'
28°00'
C'
C
M5.7
M5.3
N201
N203
mm/yr
−6 −4 −2 0 2 4 6 8
well pads
earthquake
shale gas wells
data selecting frame
reference point
distance-elevation velocity
InSAR data
Best fitting model result
Testing model results
elevation velocity (mm/yr)
distance (km)
(b) Pore Pressure
(c) von Mises Stress
kPa
1 year
3 year
6 year
depth/km
distance/km

Poroelastic stress triggered seismic activity in the Changning shale gas hydraulic fracturing region, Sichuan Basin, China

Wei Tao[1*], Renqi Lu[1*], Dengfa He[2], Jianbao Sun[1], Yuxin Bao[1,3], Yiduo Liu[4]

Guixi Yi[5,6], Yan Zhan[1], Weikang Zhang[2], Guanshen Liu[1]

1. *State Key Laboratory of Earthquake Dynamics, Institute of Geology, China Earthquake Administration, Beijing 100029, China*
2. *College of Energy Resources, China University of Geosciences, Beijing 100083, China*
3. *Seismological Bureau of Guangdong Province, Guangzhou 510070, China*
4. *Department of Earth and Atmospheric Sciences, University of Houston, Houston, TX 77204, USA.*
5. *Seismological Bureau of Sichuan Province, Chengdu 610041, China*
6. *Chengdu Institute of the Tibetan Plateau Earthquake Research, CEA, Chengdu 610041, China*

*Corresponding authors: Renqi Lu (lurenqi@163.com), Wei Tao (taowei@ies.ac.cn)

Key points:

- Pre-existing faults in the Pre-Cambrian basement of the Changning shale gas site are revealed by high-resolution reflection profiles.
- The fully coupled poroelastic stress extending a large distance in the sediment is responsible for the induced seismicity.
- The spatial-temporal evolution of Coulomb stress could trigger the moderate earthquakes of the deep basement faults.

Abstract

The recent increase in the seismic activity in the southern Sichuan Basin, China, is potentially related to shale gas hydraulic fracturing. However, the detailed mechanism of hydraulic fracturing requires further verification. In this study, high-resolution seismic profiles are used to reveal several large pre-existing faults in the basement. Based on the fully coupled poroelastic theory, we calculate the perturbing poroelastic stress field caused by hydraulic fracturing using a finite element model constrained by well-defined geological data, detailed injection data, and radar data. The results indicate that the small earthquakes are correlated with the distribution of the poroelastic stress, which is concentrated and extends a large distance along the weak stratum in the sediment beyond the fluid diffusion. Two moderate earthquakes are consistent with the increase of the Coulomb's stress in spatial-temporal evolution; thus, they are likely triggered earthquakes resulting from the reactivation of deep pre-existing faults.

Plain Language Summary

Seismic risk caused by fluid injection has become an important topic globally. Since 2014, hydraulic fracturing for gas exploitation from tight shale formations has increased rapidly in the Changning region of the southwestern Sichuan basin in China in recent years. The seismicity rate has increased to an unprecedented high level, and two moderate earthquakes occurred in 2018 and 2019, respectively. We first reveal several large pre-existing faults in the basement of the study area, and then calculate the perturbing fluid-solid fully coupled poroelastic stress field caused by hydraulic fracturing using a well-constrained finite element model. The results indicate that the widely extended poroelastic stress along the weak stratum in the sediment might be responsible for the induced small seismicity in the Changning region. Moreover, the moderate earthquakes are likely related to the triggered slip of deep pre-existing faults by poroelastic stress propagation with continual hydraulic fracturing.

Keywords: Pre-existing faults; Seismic interpretation; Hydraulic fracturing; Fully coupled poroelastic modeling; Triggered earthquake; Changning shale gas region

1. Introduction

Injection-induced seismicity cases have been reported worldwide in the recent decade. These were associated with human industrial activities, such as shale gas hydraulic fracturing, disposal of wastewater from resource extraction, and geological sequestration of waste fluids (*e.g., Bao & Eaton, 2016; Yeck et al., 2017; Ellsworth, 2013; Goebel and Brodsky, 2018; Kim et al., 2018*). Thus, it is crucial to investigate the increased risk of induced moderate earthquakes by fluid injection. In recent injection-induced earthquake studies (*e.g., Ellsworth et al., 2013, 2019; Lei et al., 2020; Hager et al., 2021*), the terms "induced" and "triggered" have different meanings and are crucial for assessing seismic hazards. Induced earthquakes occur in rock in which the pressure or stress changes as a result of the injection, and their magnitudes are consistent with the spatial dimension of the stimulated volume. In contrast, triggered earthquakes are runaway ruptures initiated by anthropogenic forcing; they grow in size beyond the bounds of the stimulated region and release tectonic strain (*McGarr et al., 2002; Ellsworth et al., 2019*). Therefore, revealing pre-existing faults and understanding the evolution of the perturbing stress field are vital for improving seismic hazard assessment and mitigation.

Shale gas development has grown rapidly in the Changning region, southwestern Sichuan Basin, China, in recent years. The local seismicity rate has increased to an unprecedented high level since 2014 (*Lei et al., 2017a, b; Meng et al., 2019; Yi et al., 2020. Long et al., 2020*). The Dec 16, 2018 Xingwen *M*s5.7 earthquake and the Jan 3, 2019 Gongxian M_s5.3 earthquake occurred in the Changning region. The two moderate earthquakes are regarded as induced earthquakes (*Lei et al., 2019*) because their centroid moment depths are 3 and 1.8 km according to the moment tensor solutions and the shale gas reservoirs of the Changning region located at a depth of 2-3 km (*He et al., 2019*). In contrast, another study suggested that the earthquakes were triggered by the reactivity of the pre-existing faults below the shale gas reservoirs (*Tan et al., 2020*) and the relocated earthquake results indicated their focal depths ranged from 6 to 9 km (*Long et al., 2020; Hu et al., 2021*). Pre-existing faults and the stress evolution are crucial to understanding this contradiction. Moreover, there are plans for significant hydraulic fracturing exploration in the Changning region in the near future. Therefore, it is necessary for seismic risk assessment to reveal the pre-existing faults in this region and understand the mechanism of hydraulic fracturing and its effect on the surrounding area.

In previous studies, the standard model of injection-induced seismicity assumes that changes in the Coulomb stress are solely the results of changes in pore pressure (*Segall & Lu, 2015*). In recent years, the effects of fully coupled poroelastic stress have been recognized (*e.g., Segall & Lu, 2015; Tao et al., 2015; Chang & Segall, 2016; Goebel & Brodsky, 2018*). The fully coupled poroelastic stress field can extend well beyond the area of fluid pressure increase in the hydraulically connected region. An indirect transfer of stress may perturb faults even without direct diffusion of fluid into the faults (*Segall & Lu, 2015*). Therefore, pre-existing faults and the effects of fully coupled poroelastic stress have to be considered to evaluate seismicity risk and assess whether earthquakes are induced or triggered by fluid injection.

In this study, we reveal pre-existing faults in the Changning region using high-resolution seismic profiles. Based on the fully coupled poroelastic theory, we use a finite element model to calculate the perturbing poroelastic stress field caused by hydraulic fracturing. The finite element model is constrained by a well-defined geological model, detailed injection data, and radar data. We simulate the evolution of the fully coupled poroelastic stress in the crust and compare it with the small seismicity distribution. We calculate the changes in Coulomb stress constrained by pre-existing faults to evaluate the relationships between hydraulic fracturing and the two moderate earthquakes.

2. Tectonic settings

The Sichuan Basin is situated near the eastern margin of the Tibetan Plateau (Figure 1a), and the study area of the Changning region is located in the southwestern Sichuan Basin (Figure 1b). Tectonically, the Changning region is at the junction of the Huaying Shan fold belt and the Daliang Shan and Dalou Shan fault-fold belts, with multistage structural deformation superimposed in different directions since the Cretaceous (*Li et al., 2011; He et al., 2019; Jiang et al., 2020*). The Daliang Shan is an active block with many active faults and frequent earthquakes (*Xu et al., 2003; He et al., 2008*). In contrast, the Dalou Mountain and Huaying Shan are relatively stable orogenic belts that developed during the Cenozoic (*Deng et al., 2013*).

Before the 2019 Changning M6.0 earthquake (Figure 1c), several moderate (M 5) earthquakes (*Lu et al., 2021*), as well as a large number of small and micro-earthquakes, occurred in the study area (*Long et al., 2020*). The seismicity rate in the Jianwu syncline, south of the Changning anticline, increased dramatically after 2014 (*Lei et al., 2017a*). Three moderate earthquakes have occurred at the Changning shale gas site since 2017 (Figure 1c). Detailed seismic studies have been carried out, such as the analysis of the focal mechanisms and the relocation of small and moderate earthquakes (*Lei et al., 2019, 2020; Yi et al., 2019, 2020; Tan et al., 2020; Yang et al., 2021; Sheng et al., 2020; Long et al., 2020; Hu et al., 2021*). Because the shale gas fields of the Petro China Company are located near the Jianwu syncline, the seismicity has been attributed to earthquakes induced by hydraulic fracturing during shale gas exploitation (*Lei et al., 2019; Meng et al., 2019; Tan et al., 2020*).

The Changning fold zone consists of the NWW-trending Changning anticline and Jianwu syncline. The strata in the Changning region are well developed (see Text S1 in the supporting information), with a Mesozoic and Paleozoic sedimentary thickness of more than 5,000 m (Figure S1). The main shale gas reservoirs in the Changning shale gas site are buried at a depth of 2500 to 3500 m in the Jianwu syncline (*Lu et al., 2021*).

3. Methodology

Two-dimensional (2-D) seismic reflection profiles revealed structural deformations of the Changning anticline and Jianwu syncline (*He et al., 2019; Lu et al., 2021*), as well as some major thrusts in the sedimentary cover. However, the basement image was not clear, and some deep thrusts were interpreted based only on the theory of fault-related folds (*Suppe, 1983; Shaw et al., 2004*). Three-dimensional (3-D) high-resolution seismic reflection data of the Changning shale gas field were collected in 2011. In this study, we present two seismic reflection profiles extracted from the 3-D seismic data (Figure 2 & Figures S3, S4). The two profiles, A-A and B-B , cross the shale gas field and are close to the epicenters of the 2018 Ms5.7 earthquake and the 2019 Ms5.3 earthquake, respectively. Both seismic profiles were converted from the time domain to the depth domain using the regional velocity model (*Wang et al., 2016*). Small-scale faults could be identified clearly in the sedimentary cover, and large faults were distinguished in the basement according to the continuity of the seismic reflectors using conventional seismic interpretation methods.

Seismic profile A-A is close to the drilling well N203 (Figure 1c) and the epicenter of the 2018 Ms 5.7 (Mw 5.2) earthquake. The centroid depth of this earthquake was reported as 3.09 km (*Lei et al., 2019*), while the focal depth was approximately 6.7 km (*Hu et al., 2021*). The scaling relations associate the earthquake size (magnitude Mw or Ms) with the fault rupture parameters, such as the surface or subsurface rupture length, rupture width, and area (*Well & Coppersmith, 1994; Leonard, 2010*). Typically, a Ms 5.0 earthquake has a rupture fault with a length of at least 2 km, according to the new empirical relationships (*Cheng et al., 2019*). Thus, the pre-existing fault that triggered a moderate earthquake should be detectable in the high-resolution 3-D reflection profile. However, no prominent fault was detected near the centroid depth. Instead, we found a basement fault near the focal depth (Figure 2a). The focal mechanism indicated that the 2018 Ms 5.7 earthquake was a typical strike-slip event (*Lei et al., 2019; Yi et al., 2019*). Our seismic interpretation suggests that the pre-existing basement faults are steep, have a normal slip component, and were active in the Neoproterozoic. Here we mapped the relocated aftershocks (*Long et al., 2020*). Most small earthquakes occurred between the Cambrian and the basement (Figure 2a), indicating that some basement faults were reactivated.

Seismic profile B-B is near the drilling well N201 (Figure 1c), and the epicenter of the 2019 Ms 5.3 earthquake was close to this profile (Figure 2b). The focal mechanism shows that the Ms 5.3 earthquake has a thrust component with some strike-slip components (*Lei et al., 2019*). Seismic interpretation indicated numerous pre-existing faults in the sedimentary cover and basement (Figure 2b); however, most were beneath the Lower Silurian and Upper Ordovician shale gas reservoirs. Different scale faults could be identified clearly in profile B-B . Only a few faults occurred in the Mesozoic strata, and some small faults were found in the Paleozoic. Many faults existed beneath the Cambrian, and many large-scale faults had developed in the basement. The centroid depth of the 2019 Ms 5.3 earthquake was 1.84 km (*Lei et al., 2019*), and the focal depth was 8.5 km (*Hu et al., 2021*). Similarly, we did not find any pre-existing faults near the centroid depth (Figure 2b) but detected many large basement faults near the focal depth. Small earthquakes occurred between the Ordovician strata and the basement, and the aftershocks were not distributed in linear clusters. The seismic interpretations support that the basement faults may have been reactivated during hydraulic fracturing of shale gas exploration.

To understand the mechanism of hydraulic fracturing, we established a 2-D finite element model of the Changning region (Figure S2) based on the fully coupled poroelastic theory (see Text S2 in the supporting information) and constrained the model by the well-defined geology model and the detailed hydraulic fracturing data in the Changning region (see Text S3 in the supporting information). We assumed saturated porous media in the Changning region and that the stresses of the rock matrix and the fluid pressure in the pore spaces (pore pressure) were mechanically coupled to manifest the stress field.

4. Results

Injecting high-pressure liquid into the shale formation results in surface deformation. To measure the surface deformation during the active periods of shale gas exploitation, we conducted a time-series analysis of the persistent scattered (PS)-InSAR data obtained from the Sentinel-1 satellite. We obtained the linear velocity field from Feb. 2015 to May 2019 (Figure 3a-left). We selected the InSAR data of profile CC' (in the brown frame in Figure 3a-left) and compared the elevation velocity profile of the InSAR data with the surface velocity of the simulation results (Figure 3a-right). The negative velocity zone in the InSAR data was caused by lateral deformation. The InSAR data show a substantial surface uplift near the wells and horizontal motion in the production period with fluid diffusion. A maximum surface elevation velocity of around 5-6 mm/yr was observed in the center of the hydraulic fracturing field relative to the adjacent region; the closer the location to the hydraulic fracturing field, the higher the elevation velocity was. Moreover, ALOS-2 interferometry showed a maximum uplift of around 120 mm in this region. We constrained the relative pressure on the well walls and the liquid injection velocity of the model by the InSAR data. The wells N203 and N201 are located northeast of the shale gas exploration region. When we compared the deformation velocity profiles of the SAR data and the modeling results, we matched the center of the hydraulic fracturing field and the source center in the 2-D model. We present several simulated surface velocity profiles and the InSAR elevation velocity profile in Figure 3a-right. We then chose the best fitting model, which was used for the subsequent analysis.

Figure 3b shows the evolution of the pore pressure. In a fluid-solid fully coupled system, the pore pressure increase in the injection zone exerts a load on the surrounding rock matrix. The deformation of the rock matrix extends farther and changes the pore pressure in the distant rock, resulting in a far-field perturbation of the poroelastic stress field. Following initial loading, the pore pressure increased rapidly around the well sites in response to the high-pressure flow injection. Within 3 years, constant hydraulic fracturing resulted in a positive pore pressure front propagating outward from the well pads through the shale formation. After 6 years of hydraulic fracturing, the pore pressure front intersected the shale formation to the stratum below with over 30 kPa. Due to permeability differences between the stratum layers, the pore pressure front extended a larger distance along the shale stratum than downward to the underlying strata (Figure 3b).

To understand the relationship between the fully coupled poroelasticity and local seismicity, we compare the distribution of the von Mises stress with the that of small seismicity. The von Mises stress is based on the shear strain energy. It is defined as

$$\sigma_M = \sqrt[2]{((\sigma_1 - \sigma_2)^2 + (\sigma_2 - \sigma_3)^2 + (\sigma_3 - \sigma_1)^2)/2} \; (1)$$

where σ_M is the von Mises stress, and $\sigma_1,\ \sigma_2,\ and\ \sigma_3$ are the first, second, and third principal stresses, respectively. In continuous media, the media yield when the von Mises stress reaches the yield strength. Therefore, the distribution of the von Mises stress can indicate the region prone to fracturing.

Our simulation results demonstrate that the von Mises stress is concentrated and extends a large distance in the stratum beneath the shale formation at depths of 3 to 5 km (Figure 3c). A relatively weak stratum exists in the strata with a low Young's modulus and high permeability due to a thick layer of sandstone and gypsum in this stratum. The fully coupled poroelastic stress extends a large distance (almost 20 km) from the well along the weak layer without fluid diffusion to this distance after six years. We projected the induced small seismicity near cross-sections BB' and AA' to the model region. As shown in Figure 3c, most small earthquakes are located between the stratum under the shale reservoir in the sediment and basement, demonstrating that the induced earthquakes were clustered beneath the shale formation in the sediment in the

Changning region. The study of the focal depth distribution suggested that the large majority of earthquakes occurred above a depth of 6 km (*Long et al., 2020*) and were associated with low-velocity anomalies (*Tan et al., 2020*). Our analysis clarifies the driving mechanism. Due to the effect of fully coupled poroelasticity, the poroelastic stress is concentrated and extends a large distance along the weak layer with high permeability and low Young's modulus in the sediment strata beyond the fluid diffusion distance. The study of the spatial footprint of the injection wells (*Goebel & Brodsky, 2018*) suggested a steady decay for sites with strong poroelastic coupling above the basement and an abrupt decay for pressure-dominated sites below the basement. Our results clarify the mechanism of poroelastic coupling and demonstrate a contrast in the poroelastic stresses, i.e., strong coupling in the sediment and relative weak coupling in the basement. Therefore, the effect of the fully coupled poroelasticity is likely responsible for injection-induced seismicity at large distances from the wells.

5. Discussion and conclusions

Our seismic interpretation indicates the existence of many pre-existing faults in our study region (Figure 2). To evaluate the potential seismic risk, we assessed the Coulomb stresses of the faults to determine the effect of the perturbation stress field resulting from hydraulic fracturing on the potential reactivation of pre-existing faults.

The Coulomb failure criterion is widely used to characterize changes in the frictional slip along a pre-existing incipient fault plane (*e.g., King et al., 1994; Cocco & Rice, 2002*). The change in the Coulomb stress (CFS) is defined as:

$$CFS = \ \sigma_s + \mu(\ \sigma_n + \ P) \ (2)$$

where $_s$ is the incremental change in the shear stress (in the positive slip direction); $_n$ is the incremental change in the fault-normal stress (extension-positive); P is the incremental change in pore pressure; μ is the coefficient of friction, which ranges from 0.6 to 0.85 for most rocks (*Byerlee, 1978, 1992; Harris, 1998*). We use the median value 0.7 in this study.

The probability of inducing/triggering an earthquake at a distance depends on the presence and number of faults and the amplitude of stress perturbation (*Goebel & Brodsky, 2018*). Our seismic interpretation indicated several pre-existing faults in the sedimentary cover and basement in the study region. Hu et al. (2021) relocated the 2018 Xingwen Ms 5.7 earthquake and the 2019 Gongxian Ms 5.3 earthquake using a double-difference algorithm and obtained focal depths of 6.76 km and 8.45 km, respectively. A series of thrust faults with ~ 45º dip angles were revealed in the basement near the Gongxian Ms 5.3 earthquake location, and several faults with ~65º angles dip angle were revealed near the Xingwen Ms 5.7 earthquake location (Figure 2). We calculated the spatial-temporal evolution of the ΔCFS according to the dip angles and properties of the faults surrounding the two events (Figure 4). Due to the low permeability of rocks, a direct hydraulic connection between the wells and the large faults could not have developed within a few years. However, the results demonstrate positive ΔCFS regimes extending from the well pads to the surrounding area. After 3 years of hydraulic fracturing, the positive ΔCFS front (24 kPa) extends a few kilometers laterally along the shale formation (Figure 4a). After 6 years, relative to the faults with 45^{o} (Figure 4b) or 65^{o} dip angles (Figure 4c), the positive ΔCFS front (24 kPa) spreads more than 10 km laterally and further across the stratum boundary below, reaching depths of 6 to 8 km in the basement. The focal depth of the Xingwen Ms 5.7 earthquake is located within the positive ΔCFS front region of 24 kPa (Figure 4c), and that of the Gongxian Ms 5.3 earthquake is located within the positive ΔCFS front region of 16 kPa (Figure 4b). Since the direction of the maximum principal stress axis in the Jianwu flat syncline is almost horizontal (a slope of 5.7±3.3°) with an azimuth of 117°, the intermediate principal stress axis is almost horizontal, and the minimum principal stress axis is nearly vertical (*Lei et al., 2020*). Therefore, both strike-slip and reverse faults of a favorable orientation could be easily reactivated in this tectonic stress background. Moreover, a previous study suggested that increases in 5 kPa in the CFS are typically associated with the triggering of large events (M>5.5) (*Cochran et al., 2004*). Increases in the CFS of dozens of kPa occurred near the focal location of the two moderate earthquakes due to hydraulic fracturing. Therefore, the two moderate earthquakes in the Changning region were likely triggered earthquakes resulting from the reactivation of pre-existing faults in the basement.

There are plans for significant hydraulic fracturing exploration in the southwestern Sichuan Basin in the near future. If the hydraulic fracturing operation were sustained for 9 years, the ΔCFS front exceeding 24 kPa would extend to a depth of 10 km in the basement (Figure 4d), and the risk of reactivating pre-existing faults would be relatively high. Therefore, a traffic-light protocol study is required to mitigate the seismic hazards during hydraulic fracturing. A process-based approach to understanding and managing triggered seismicity is required (*Hager et al., 2021*).

In conclusion, our study suggests the following. (1) Seismic interpretation indicates several pre-existing faults in the sedimentary cover and the basement in the Changning region; most large faults are located beneath the Lower Silurian and Upper Ordovician shale gas reservoirs. (2) Due to the effect of the fully coupled poroelasticity, the poroelastic stress is concentrated and extends a large distance in the weak strata with high permeability and low Young's modulus in the sediment beyond the fluid diffusion. This mechanism is likely responsible for the injection-induced seismicity at large distances from the wells beneath the gas reservoir in the Changning region. (3) The spatiotemporal evolution of the ΔCFS demonstrates that the Xingwen Ms 5.7 and the Gongxian Ms 5.3 earthquakes were triggered by poroelastic stress propagation resulting from the reactivation of deep pre-existing faults. The risk of reactivating pre-existing faults increases with long-term sustained hydraulic fracturing.

Acknowledgments

This work is supported by the National Nonprofit Fundamental Research Grant of China, Institute of Geology, China, Earthquake Administration [grant numbers IGCEA2103, IGCEA1919, IGCEA2007]; National Natural Science Foundation of China [grants number 42074118]. Many of the ideas presented in this paper benefited from discussion with Professor Zhengkang Shen and Lifeng Wang. We thank the Petro China providing the high-resolution seismic reflection profiles to support this study.

Competing interests

The authors declare no competing interests.

Data Availability Statement

The seismicity events from May 1, 2017 to August 31, 2018, from December 16, 2018 to January 7, 2019 and from June 17 to July 4, 2019 in the Changning anticline are available through Long et al., 2020. Earthquake focal mechanisms were taken from previous published articles (*Lei et al., 2017a, 2019; Liu & Zahradnik, 2020*). The two high-resolution seismic reflection profiles were provided courtesy of the Southwest Oil and Gas Field Company, Petro China (Figures S3 & S4). They are allowed to be released to the public for the non-profit scientific study. Everyone can find the un-interpreted seismic reflection profiles in the supplemental material file.

References

Bao, X., & Eaton, D. W. (2016). Fault activation by hydraulic fracturing in western Canada. *Science*, 354(6318), 1406–1409. https://doi.org/10.1126/science.aag2583

Byerlee, J. D. (1992). The change in orientation of subsidiary shears near faults containing pore fluid under high pressure. *Tectonophysics*, 211, 295-303. https://doi.org/10.1016/0040-1951(92)90066-F

Byerlee, J. D. (1978). Friction of rocks. *pure and applied geophysics*, 116, 615-626. https://doi.org/10.1007/978-3-0348-7182-2_4

Chang, K. W., & Segall, P. (2016). Injection-induced seismicity on basement faults including poroelastic stressing. *Journal of Geophysical Research: Solid Earth*, 121, 2708-2726. https://doi.org/10.1002/2015JB012561

Cheng, J., Rong, Y., Magistrale, H., Chen, G., & Xu, X. (2019). Earthquake Rupture Scaling Relations for Mainland China. *Seismological Research Letters*, 91, 248-261. https://doi.org/10.1785/0220190129

Cocco, M., Rice, & J. R. (2002). Pore pressure and poroelasticity effects in Coulomb stress analysis of earthquake interactions. *Journal of Geophysical Research: Solid Earth*, 107(B2), 2030. https://doi.org/10.1029/2000JB000138

Cochran, E. S., Vidale, J. E., & Tanaka, S. (2004). Earth tides can trigger shallow thrust fault earthquakes. *Science*, 306, 1164-1166. https://doi.org/10.1126/science.1103961

Deng, B., Liu, S., Wang, G., & Li, Z. W. (2013). Cenozoic uplift and exhumation in southern Sichuan basin-evidence from low-temperature thermochronology. *Chinese Journal of Geophysics*, 56(6), 1958-1973 (in Chinese with English abstract). https://doi.org/10.6038/cjg20130618

Domenico, P. A., & Schwartz, F. W. (1998). Physical and chemical hydrogeology, P171. 2nd ed. John Wiley & Sons, New York.

Ellsworth, W. L., Giardini, D. Townend, J., Ge, S., & Shimamoto, T. (2019). Triggering of the Pohang, Korea, Earthquake (Mw 5.5) by Enhanced Geothermal System Stimulation. *Seismological Research Letters*. https://doi.org/10.1785/0220190102

Ellsworth, W. L. (2013). Injection-induced earthquakes. *Science*, 341, 6142, 1225942. https://doi.org/10.1126/science.1225942

Goebel, T. H. W., & Brodsky, E. E. (2018). The spatial footprint of injection wells in a global compilation of induced earthquake sequences, *Science,* 361, 6405, 899-904. https://doi.org/10.1126/science.aat5449

Hager, B. H., Dieterich, J., Frohlich, C., Juanes, R., Mantica, S., Shaw, J. H., Bottazzi, F., Caresani, F., Castineira, D., Cominelli, A., Meda, L., Osculati, M., Petroselli S., & Plesch, A. (2021). A process-based approach to understanding and managing triggered seismicity. *Nature*, 595, 7869, 684-689. https://doi.org/10.1038/s41586-021-03668-z

Harris, R. A. (1998). Introduction to special section: Stress triggers, stress shadows, and implications for seismic hazard. *Journal of Geophysical Research: Solid Earth*, 103, 24,347-24,358. https://doi.org/10.1029/98JB01576

He, H. L., Ikeda, Y., He, Y. L., Togo, M., Chen, J., Chen, C. Y., Tajikara, M., Echigo T., & Okada. S. (2008). Newly-generated Daliangshan Fault Zone-Shortcutting on the central section of Xianshuihe-Xiaojiang fault system. *Science in China Series D: Earth Sciences*, 51(9), 1248-1258. https://doi.org/10.1007/s11430-008-0094-4

He, D. F., Lu, R., Huang, H., Wang, X. S., Jiang, H., & Zhang, W. (2019). Tectonic and geological setting of the earthquake hazards in the Changning shale gas development zone, Sichuan Basin, SW China. *Petroleum Exploration and Development*, 46(5), 1051-1064. https://doi.org/10.1016/S1876-3804(19)60262-4

Hu, X. P., Cui, X. F., Zhang, G. W., Wang, H.J., Zang, A., Shi, B. X., & Jiang, D. W. (2021). Analysis on the mechanical causes of the complex seismicity in Changning area, China. *Chinese Journal of Geophysics*, 64(1), 1-17 (in Chinese with English abstract). https://doi.org/10.6038/cjg2021O0232

Jiang, D., Zhang, S., & Ding, R. (2020). Surface deformation and tectonic background of the 2019 Ms 6.0 Changning earthquake, Sichuan Basin, SW China. *Journal of Asian Earth Sciences*. https://doi.org/10.1016/j.jseaes.2020.104493

King, G. C. P., Stein, R. S., & Lin, J. (1994). Static stress changes and the triggering of earthquakes. *Bulletin of the Seismoogical Society of America*, 84, 935-953. https://doi.org/10.1016/0148-9062(95)94484-2

Lei, X., Huang, D., Su, J., Jiang, G., Wang, X., Wang, H., Guo, X., & Fu, H. (2017a). Fault reactivation and earthquakes with magnitudes of up to Mw4. 7 induced by shale-gas hydraulic fracturing in Sichuan Basin, China. *Scientific Reports*, 7(1), 7971-7912. https://doi.org/10.1038/s41598-017-08557-y

Lei, X., Ma, S., Wang, X., & Su, J. (2017b). Fault-valve behavior and episodic gas flow in over-pressurized aquifers – evidence from the 2010 Ms5.1 isolated shallow earthquake in Sichuan Basin, China. *Progress in Computational Fluid Dynamics*: 1-12. https://doi.org/10.1504/PCFD.2017.081714

Lei, X., Su, J., & Wang, Z. (2020). Growing seismicity in the Sichuan Basin and its association with industrial activities, *Science China (Earth Sciences)* 11. https://doi.org/10.1007/s11430-020-9646-x

Lei, X., Wang, Z., & Su, J. (2019). The December 2018 ML 5.7 and January 2019 M_L 5.3 Earthquakes in South Sichuan Basin Induced by Shale Gas Hydraulic Fracturing. *Seismological Research Letters*, 90, 1099-1110. https://doi.org/10.1785/0220190029

Leonard, M. (2010). Earthquake fault scaling: Self-consistent relating of rupture length, width, average displacement, and moment release. *Bulletin of the Seismological Society of America*, 100, 1971-1988. https://doi.org/10.1785/0120090189

Li, S. J., Li, J. M., Zhou, Y., Wo, Y. J., & Wang, X. W. (2011). Fission track evidence for Mesozoic-Cenozoic uplifting in the southeastern margin of Sichuan basin. *Acta Petrologica Et Mineralogica*, 30(2), 225-233 (in Chinese).

Liu, J., & Zahradník, J. (2020). The 2019 MW 5.7 Changning earthquake, Sichuan Basin, China–a shallow doublet with different faulting styles. *Geophysical Research Letters*, e2019GL085408. https://doi.org/10.1029/2019GL085408

Long, F., Zhang, Z. W., Qi, Y. P., Liang, M. J., Ruan, X., Wu, W. W., Jiang, G. M., & Zhou, L. Q. (2020). Three dimensional velocity structure and accurate earthquake location in Changning-Gongxian area of southeast Sichuan. *Earth and Planetary Physics*, 4(2), 163-177. https://doi.org/10.26464/epp2020022

Lu, R., He, D., Liu, J.-Z., Tao, W., Huang, H., Xu, F., & Liu, G. (2021). Seismogenic Faults of the Changning Earthquake Sequence Constrained by High-Resolution Seismic Profiles in the Southwestern Sichuan Basin, China. *Seismological Research Letters* , 92, 3757-3766, https://doi.org/10.1785/0220200302.

McGarr, A., Simpson, D., & Seeber, L. (2002). Case histories of induced and triggered seismicity, in International Handbook of Earthquake and Engineering Seismology 81A, 647–661, Academic Press, San Francisco, Calif.

Meng, L., McGarr, A., Zhou, L., & Zang, Y. (2019). An Investigation of Seismicity Induced by Hydraulic Fracturing in the Sichuan Basin of China Based on Data from a Temporary Seismic Network. *Bulletin of the Seismological Society of America*, 109, 348-357. https://doi.org/10.1785/0120180310

Ren, R., Qian, B., Zhang, J., Zhuo, Z., & Qio, L. (2015). Practice and understanding of industrial fracturing for shale gas of Longmaxi Formation in Changning region. *Oil Drilling & Production Technol*ogy, 37, 96-99 (in Chinese with English abstract). https://doi.org/CNKI:SUN:SYZC.0.2015-04-032

Segall, P. (1989). Earthquakes triggered by fluid extraction, *Geology* 17(10), 942-946. https://doi.org/10.1130/0091-7613

Segall, P., Grasso, J.-R., & Mossop, A. (1994). Poroelastic stressing and induced seismicity near the Lacq gas field, southwestern France. *Journal of Geophysical Research* 99(B8), 15,423-15,438. https://doi.org/10.1029/94JB00989

Segall, P., & Lu, S. (2015). Injection-induced seismicity: poroelastic and earthquake nucleation effects. *Journal of Geophysical Research: Solid Earth*, 120, 5082-5103. https://doi.org/10.1002/2015JB012060

Shaw, J. H., Connors, C. D., & Suppe, J. (2004). Seismic interpretation of contractional fault-related folds: An AAPG seismic atlas 53, American Association of Petroleum Geologists.

Sheng, M., Chu, R., Ni, S., Wang, Y., Jiang, L., & Yang, H. (2020). Source parameters of three moderate size earthquakes in Weiyuan, China, and their relations to shale gas hydraulic fracturing. *Journal of Geophysical Research: Solid Earth*, 125, e2020JB019932. https://doi.org/10.1029/2020JB019932

Suppe, J. (1983). Geometry and kinematics of fault-bend folding. *American Journal of science*, 283(7), 684-721. https://doi.org/10.2475/ajs.283.7.684

Tan, Y., Hu, J., Zhang, H., Chen, Y., Qian, J., Wang, Q., Zha, H., Tang, P., & Nie, Z. (2020). Hydraulic Fracturing Induced Seismicity in the Southern Sichuan Basin Due to Fluid Diffusion Inferred From Seismic and Injection Data Analysis. *Geophysical Research Letters*, 47. https://doi.org/10.1029/2019GL084885

Tao, W., Masterlark, T., Shen, Z., & Ronchin, E. (2015). Impoundment of the Zipingpu Reservoir and Triggering of the 2008 Mw 7.9 Wenchuan Earthquake, China. *Journal of Geophysical Research: Solid Earth*, 120. https://doi.org/10.1002/2014JB011766

Tapponnier, P., Xu, Z.Q., Roger, F., Meyer, B., Arnaud, N., Wittlinger, G., & Jing, S. Y. (2001). Oblique stepwise rise and growth of the Tibet Plateau. *Science*, 294, 5547, 1671-1677. https://doi.org/10.1126/science.105978

Wang, H. F. (2000). Theory of Linear Poroelasticity: With Applications to Geomechanics and Hydrogeology. Princeton Univ. Press, Princeton and Oxford.

Wang, Y. M., Huang, J. L., Wang, S. F., Dong, D. Z., Zhang, C. C., & Guan, Q. Z. (2016). Dissection of two calibrated areas of the Silurian Longmaxi Formation, Changning and Jiaoshiba, Sichuan basin. *Natural Gas Geoscience*, 27(3), 423-432 (in Chinese with English abstract).

Wells, D., & Coppersmith, K. (1994). New empirical relationships among magnitude, rupture length, rupture width, rupture area, and surface displacement. *Bulletin of the Seismoogical Society of America*, 84, 974-1002. https://doi.org/10.1007/BF00808290

Xu, X. W., Wen, X. Z., Zheng, R. Z., Ma, W., Song, F., Yu, G. (2003). Pattern of latest tectonic motion and its dynamics for active blocks in Sichuan-Yunnan region, *China. Science in China Series D: Earth Sciences*, 46(2), 210-226. https://doi.org/10.1360/03dz0017

Yang, Y. H., Hu, J. C., Chen, Q., Lei, X. L., Zhao, J., Li, W., Xu, R., Chun-Ying, C. (2021). Shallow Slip of Blind Fault associated with the 2019 Ms 6.0 Changning Earthquake in Fold-and-Thrust Belt in Salt Mines of Southeast Sichuan, China. *Geophysical Journal International*, 224, 909-922. https://doi.org/10.1093/gji/ggaa488

Yeck, W. L., Hayes, G. P., Mcnamara, D. E., Rubinstein, J. L., Barnhart, W. D., Earle, P. S., Benz H. M. (2017). Oklahoma experiences largest earthquake during ongoing regional wastewater injection hazard mitigation efforts. *Geophysical Research Letters*, 44, 711-717. https://doi.org/10.1002/2016GL071685

Yi, G., Long, F., Liang, M., Zhao, M., & Wang, S. (2020). Geometry and tectonic deformation of seismogenic structures in the Rongxian-Weiyuan-Zizhong region, Sichuan Basin: insights from focal mechanism solutions. *Chinese Journal of Geophysics*, 63(9), 3275-3291 (in Chinese with English abstract). https://doi.org/10.6038/cjg2020O0095

Yi, G., Long, F., Liang, M., Zhao, M., Wang, S., Gong, Y., Qiao, H., & Su, J. (2019). Focal mechanism and seismogenic structure of the 17 June 2019 Ms6.0 Sichuan Changning earthquake sequence. *Chinses Journal of Geophysics*, 62, 1-16 (in Chinese with English abstract). https://doi.org/10.6038/cjg2019N0297.

Figure captions

Figure 1. Seismicity distribution in the Changning region, southern Sichuan Basin. (a) Simplified tectonic map of the Tibetan Plateau region. Our study area is located in the southern Sichuan Basin (modified from *Tapponnier et al., 2001*). (b) Topographic map of the Sichuan Basin and the eastern Tibetan Plateau. (c) Geological and seismological background. The solid red lines are fault surface traces. The colored beach balls illustrate the epicenters of M 5.0 events in recent years (*Lei et al., 2017a, 2019; Liu & Zahradnik, 2020; Hu et al., 2021*). The black dots indicate induced seismicity events from May 1, 2017 to August 31, 2018; the blue dots indicate induced seismicity events from December 16, 2018 to January 7, 2019; the red dots indicate seismicity events from June 17 to July 4, 2019 in the Changning anticline (*Long et al., 2020*). The rectangular white box shows the shale gas site in the Changning region.

Figure 2. Seismic interpretation and structural model of profile A-A and B-B' with (up) and without (down) the seismic profile in the background. The yellow dots mark the major boundaries of the sedimentary layers. The solid purple lines denote pre-existing faults, and the dashed lines are inferred faults. The blue circles are relocated earthquakes from Dec 16, 2018 to Jan 7, 2019 (*Long et al., 2020*). The red stars show the centroid depths of the Ms 5.7 earthquake in (a) and the Ms 5.3 earthquake in (b) (*Lei et al., 2019*), and the yellow stars show the focal depths (*Hu et al., 2021*). The shale gas reservoirs are the green layers located in the Lower Silurian and Upper Ordovician in the study area.

Figure 3. (a) Linear velocity field from InSAR data analysis and simulated vertical deformation velocity profile. Left: PS-InSAR linear velocity field in ascending orbit obtained from Sentinel-1 radar data at the Changning shale gas site from Feb. 2015 to May 2019. The black dots indicate the shale gas wells in the Changning region obtained from field investigations; the triangles indicate the well pads. Right: elevation velocity profile in ascending orbit and the simulated surface elevation velocities of the testing model. (b) Spatial evolution of pore pressure one, three, and six years after hydraulic fracturing. The range of the pore pressure is 0 kPa to $>$ 24.0 kPa. (c) Spatial evolution of the von Mises stress one, three, and six years after hydraulic fracturing. The range of the von Mises stress is 0 to $>$ 12 kPa. The yellow star denotes the focal position of the Ms 5.7 earthquake, and the light blue star denotes that of the Ms 5.3 earthquake (*Hu et al., 2021*). The black lines show the interpreted faults in this study. The grey lines show the strata structure. The blue dots show the induced seismicity from May 1, 2017 to Aug 31, 2018 and from Dec 16, 2018 to Jan 7, 2019.

Figure 4. Spatial evolution of Coulomb stress after hydraulic fracturing.

The stresses are plotted from 0 kPa to greater than 24.0 kPa using the color legend. The yellow star denotes the focal position of the Xingwen Ms 5.7 earthquake, and the blue star denotes the Ms 5.3 earthquake (*Hu et al., 2021*). The black lines are the faults interpreted from the seismic profile AA' and BB' in this study. The grey lines show the strata structure. The blue dots show the induced seismicity from May 1, 2017 to Aug 31, 2018 and from Dec 16, 2018 to Jan 7, 2019.